Spectral Analysis and Diagnosis of Nonlinear Interactions of Large-Scale Moving Waves at 200 mb in the GLAS General Circulation Model

TSING-CHANG CHEN AND HAL G. MARSHALL

Department of Earh Sciences, Iowa State University, Ames 50011

J. SHUKLA

NASA/Goddard Space Flight Center, Laboratory for Atmospheric Sciences, Greenbelt, MD 20771 and Department of Meteorology, Massachusetts Institute of Technology, Cambridge 02139

(Manuscript received 29 April 1980, in final form 20 October 1980)

ABSTRACT

Wavenumber-frequency spectral analysis of a 90-day winter (15 January–14 April) wind field simulated by a climate experiment of the GLAS (Goddard Laboratory for Atmospheric Sciences) atmospheric circulation model is made using the space-time Fourier analysis which is modified with Tukey's numerical spectral analysis. Computations are also made to examine the nonlinear interactions of model wave disturbances in the wavenumber-frequency domain linear interactions. Results are compared with observation, especially Kao and Lee's (1977) study.

It is found that equatorial easterlies do not show up in this climate experiment at 200 mb. The zonal kinetic energy and momentum transport of stationary waves are too small in the model's Northern Hemisphere. The wavenumber and frequency spectra of the model are generally in good agreement with observation. However, some distinct features of the model's spectra are revealed. The wavenumber spectra of kinetic energy show that the eastward moving waves of low wavenumbers have stronger zonal motion while the eastward moving waves of intermediate wavenumbers have larger meridional motion compared with observation. Furthermore, the eastward moving waves show a band of large spectral value in the medium-frequency regime. The frequency spectra in the high-frequency regime decrease faster than observation as frequency increases. The scheme proposed by Kao and Lee for the contribution to kinetic energy spectra by nonlinear interactions in middle latitudes is not applicable over the whole model globe because of the disappearance of equatorial easterlies. The contribution to momentum flux spectra by nonlinear interactions in Northern Hemisphere middle latitudes is similar to that of kinetic energy spectra. The primary nonlinear interactions of kinetic energy and momentum flux are contributed by those between mean zonal flow and long and medium waves with low and medium frequencies. The stationary waves do not play a significant role in the nonlinear interactions as found in observation.

1. Introduction

The development of the general circulation model (GCM) in the past two decades has reached the step where the GCM is not only used to simulate the atmospheric circulation, but also employed to make medium-range forecasts and long-term climate study. The simulation of the GCM is conventionally verified against the long-term averaged spatial distribution of observed atmospheric circulation. In fact, numerous observational studies demonstrate that the life cycle of the atmospheric disturbances vary from about a week for cyclone waves to several weeks for planetary waves. Besides the evaluation of the GCM simulation in the space domain, it seems logical to assess the GCM simulation in the time domain, too.

In order to accomplish the second goal, Hayashi and Golder (1977) and Hayashi (1974) applied the lag-correlation method to make the space-time spectral analysis of the wave disturbances in midlatitudes and tropics of the GCM of the Geophysical Fluid Dynamics Laboratory (GFDL). The spectral analysis with a lag-correlation method was also employed by Pratt (1979) to analyze the midlatitude disturbances of the GCM of the National Center for Atmospheric Research (NCAR). Tsay (1974b), then, used the space-time Fourier analysis proposed by Kao (1968) to examine the tropical disturbances of the NCAR GCM.

The technique of the aforementioned spectral analysis in space and time can be classified into two methods: space-time spectral analysis (Hayashi, 1971) and space-time Fourier analysis (Kao, 1968). The former uses a lag-correlation method, while the latter uses a direct Fourier transform method. Tsay (1974a) and Pratt (1976) show these two methods are equivalent at a discrete frequency, if a frequency smoothing is applied. Recently, Kao and Lee (1977) revised Kao's original scheme by intro-

0027-0644/81/050959-16$08.00

ducing Tukey's (1967) spectral analysis technique to make extensive spectral analysis of atmospheric disturbances.

In this paper, we have carried out a diagnostic analysis of each term in the imaginary part of kinetic energy equation and compare the result with the similar computations from observation reported by Kao and Lee (1977, hereafter referred to as KL).

The detailed structure of the GLAS atmospheric circulation model is described in detail by Halem *et al.* (1979). It is a 9-level primitive equation model in σ-coordinate system. The grid system is 4° latitude × 5° longitude. The model contains a hydrological cycle, parameterization of subgrid-scale cumulus convection and orography. The radiation computation includes the calculated cloud and water vapor distribution. Arakawa's (1966) scheme is applied to treat the horizontal advections. Space time spectra of geopotential height simulated by this model are described by Straus and Shukla (1981).

Data analyzed in this study are condensed from a 4-month climate experiment (D122) using the NMC analysis of 1 January 1975 as initial field. The history output data for every 12 h over a period of 90 days starting from 0000 GMT 15 January 1975, are used. The data of the first 15 days in this climate experiment are not used to avoid the transition period.

The current study consists of two parts: space-time spectral analysis and diagnosis of the nonlinear interactions of largescale moving waves. The discussion of these two parts is presented respectively in Sections 2 and 3.

2. Spectral analysis

a. Method

The analysis of wavenumber-frequency spectra in this study follows KL's procedure in which they apply the numerical spectral analysis of Tukey (1967) to Kao's original space-time Fourier analysis (Kao, 1968). The detailed procedure of computations can be found in KL. However, a brief summary of the modified Kao's scheme should sufficiently serve the purpose of illustration. Suppose an atmospheric variable $q(\lambda, t)$ be a real single-valued function which is piecewise continuous in an interval $(0, 2\pi)$ for both longitudinal λ and time t. The complex Fourier coefficients of this atmospheric variable, $Q(k, \pm n)$, can be evaluated by

$$Q(k, \pm n) = \frac{1}{4\pi^2} \int_0^{2\pi} \int_0^{2\pi} q(\lambda, t) e^{i(k\lambda \pm nt)} ds dt, \quad (1)$$

where k and n are wavenumber and frequency, respectively. $-n$ represents the eastward moving waves, while $+n$ is westward.

The double Fourier transform is carried out in two steps. It is evaluated first in the space domain

$$Q_q(k, t) = \frac{1}{2\pi} \int_0^{2\pi} q(\lambda, t) e^{ik\lambda} d\lambda. \quad (2)$$

The wavenumber-frequency Fourier coefficients are calculated by performing the Fourier transform of wavenumber Fourier coefficients, $Q_q(k, t)$,

$$Q(k, \pm n) = \frac{1}{2\pi} \int_0^{2\pi} Q_q(k, t) e^{\pm int} dt. \quad (3)$$

Tukey's numerical spectral analysis is applied after $Q_q(k, t)$ is obtained from (2). Let us express

$$Q(k, \pm n) = Q_r(k, \pm n) + iQ_i(k, \pm n),$$

where Q_r and Q_i are the real and imaginary parts of Q, respectively. The wavenumber-frequency spectrum can be calculated by

$$E_{pq}(k, \pm n) = 2[P_r(k, \pm n)Q_r(k, \pm n) + P_i(k, \pm n)Q_i(k, \pm n)], \quad (4)$$

where $P(k, \pm n) = P_r(k, \pm n) + iP_i(k, \pm n)$ is the Fourier coefficient of a variable $p(\lambda, t)$. $E_{pq}(k, \pm n)$ is a power spectrum if $p(\lambda, t) = q(\lambda, t)$, while $E_{pq}(k, \pm n)$ is the cospectrum of p and q if $p(\lambda, t) \neq q(\lambda, t)$.

b. Latitudinal distributions of mean zonal velocity, kinetic energy of stationary and transient waves, and meridional transport of westerly momentum

The linear theory of wave motions shows that the behavior of waves critically depends upon the zonal mean state. In order to obtain some background of the zonal mean flow and wave motions of the GLAS model at 200 mb, the latitudinal distributions of zonal mean velocity, kinetic energy and meridional transport of westerly momentum of stationary ($n = 0$) and transient waves ($n \neq 0$) waves at this level are shown in Fig. 1a. The observations extracted from various studies for the period from December to February are shown in Fig. 1b to verify the simulation of the GLAS model.

The zonal mean wind of this climate run is close to the observation, except the equatorial easterlies disappear. In fact, the examination of 500 mb zonal mean wind in this climatological experiment does not show the disappearance of easterlies in the model tropics.

The model kinetic energies of the transient waves of zonal and meridional velocities, K_{tu} and K_{tv}, are very much larger than their counterparts of stationary waves, K_{su} and K_{sv}. The observational K_{su} peaks at the equator and at 35°N and has a larger value than the model's. It is obvious that the stationary waves are not well simulated in the model.

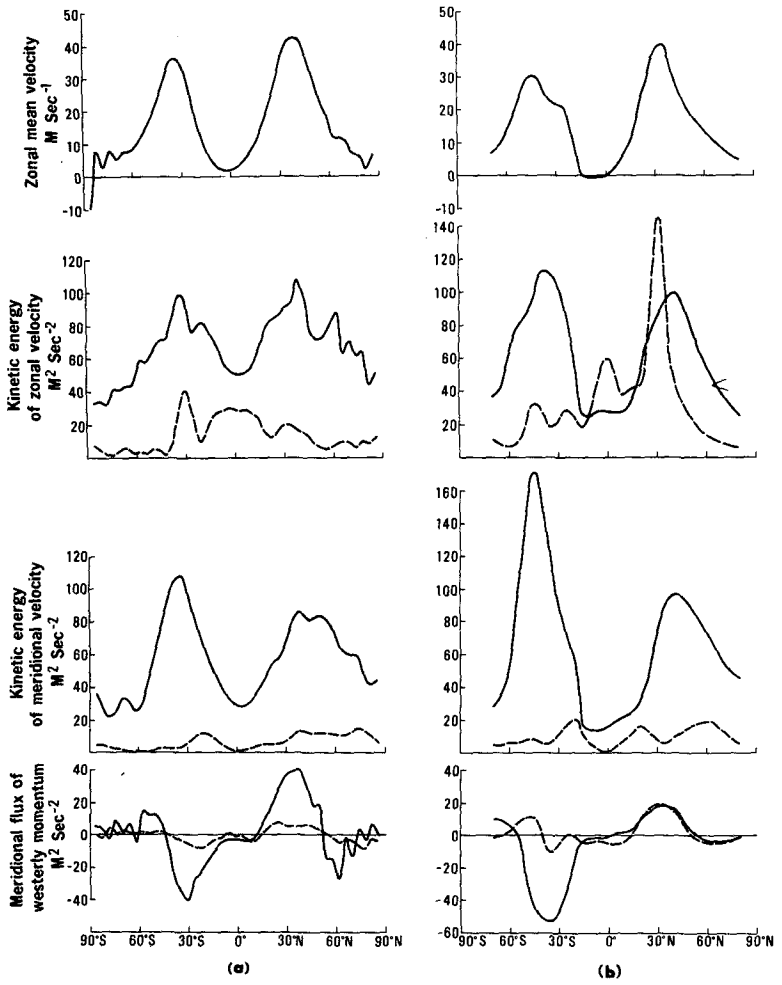

FIG. 1. Latitudinal distribution of zonal mean velocity, kinetic energy of zonal and meridional velocities of stationary and transient waves, and meridional transport of westerly momentum at 200 mb. (a) GLAS model and (b) observation from various sources. The observations north of 20°S come from KL, while south of 15°S are from the EØLE study in which zonal mean velocity and kinetic energy are drawn from Morel and Desbois (1974), and momentum transport from Webster and Curtin (1974). The solid line denotes transient waves, while the dashed line represents stationary waves.

The comparison of the kinetic energies of stationary and transient waves between the GLAS model and the observation at the 200 mb level shows that the smaller eddy kinetic energy of the model is due mainly to the zonal motion of stationary waves.

Both K_{tu} and K_{tv} have maximum values occurring at the same locations of the maximum zonal mean flow in the Southern and Northern Hemisphere (hereafter referred as SH and NH). The same situation occurs in the observation. The model maximum values of K_{tv} in the SH are much smaller than observational values. The observational kinetic energy of the transient waves is almost equally distributed in K_{tu} and K_{tv} in the NH (KL, 1977). This equal partition of K_{tu} and K_{tv} does show in the model to some extent. It should be also noted that the model K_{tu} and K_{tv} are larger than observational values in the tropics.

The latitudinal distribution of meridional transport of westerly momentum displayed in Fig. 1 shows that the model transport is equatorward in the regions north of 40°N and south of 40°S, and is poleward in the global belt between 40°N and 40°S. The meridional transport of westerly momentum in the model is mainly contributed by the transient waves. The contribution from the stationary waves is in phase constructively with the transient waves. The meridional transports of westerly momentum by stationary and transient waves in the observational study are about the same in the NH, while

the latter is dominant in the SH. The comparison of the westerly momentum transport between the GLAS model and the observational study shows that the transport is too strong by model transient waves and too weak by model stationary waves in the NH. In addition, the momentum transport by the model transient waves in the SH is slightly weaker than observational values.

It has long been well known that eddy kinetic energy is too small and eddy transport of momentum is too weak in the numerical general circulation models. Manabe *et al.* (1970) and Wellck *et al.* (1971) demonstrate that the increasing of the horizontal resolution of numerical general circulation can enhance the magnitude of eddy energies and energy conversions. It could be that the increasing of horizontal resolution may well be one of the possible ways to improve the simulation of stationary waves in the GLAS atmospheric circulation model. In fact, it has also long been realized that stationary waves are generally determined by the forcing of topography and stationary heat sources. The sophisticated general circulation models usually have realistic orography, even though it is smoothed. The increase of horizontal resolution, of course, can make the topography more realistic. The stationary heat sources must depend on the treatment of diabatic heating. In other words, the refinement of model diabatic heating scheme could be another important factor to improve the simulation of stationary waves.

c. *Wavenumber and frequency spectra of zonal and meridional kinetic energy*

In order to shed light on the wave characteristic of the GLAS model in space, the wavenumber spectral analysis is made. The wavenumber kinetic energy spectra of zonal and meridional motions are displayed in Fig. 2.

The zonal kinetic energy spectra show that the eastward moving waves have larger energy than the westward moving waves. However, the energies of these two classes of waves becomes closer, especially in the high wavenumber regime, as the equator is approached. The contrast of zonal kinetic energies between the eastward and westward waves is consistent with KL's study. The close comparison between the GLAS model and KL's observational result shows that the eastward moving waves of the model's low wavenumber regime, which possesses most of the wave energy, have larger energy content than KL values. In contrast, the model's westward moving waves have less energy than the KL values. It is interesting to note that the zonal kinetic energy of both eastward and westward waves at the equator is larger than that of KL.

Both the observational and model kinetic energy of zonal motion in the SH shown in Section 2a are mainly due to the transient waves. Desbois (1975) also shows that the zonal kinetic energy spectrum at 45°S decreases monotonically as wavenumber increases. The eastward moving waves may have higher energy content. Since Desbois' finding does not appear in this energy spectra at 38°S shown in Fig. 2a, we could infer that the zonal kinetic energy of model eastward moving wave of low wavenumber regime may be smaller in the SH middle latitudes.

The zonal kinetic energy of the model stationary wave one becomes dominant at 18 and 2°N. Krishnamurti (1971) and Krishnamurti *et al.* (1973) show that wave one, associated with the east-west circulation at 200 mb over the tropics, possesses the most significant part of wave energy and is quasi-stationary. This particular feature of wave one in the tropics is also confirmed recently by Chen (1980) and shown very clearly in KL's result. Compared with KL's result, the zonal kinetic energy of this wave in the equatorial area of the GLAS model is still too weak.

In the high wavenumber regime, Tenenbaum (1976) has shown that the overall NH kinetic energy spectrum of the GISS model has a slope of -2.6 between waves 8 and 15. Fig. 2a shows that the -3 power law is applicable in high and middle latitudes. However, the slope of the zonal kinetic energy spectrum in the high wavenumber regime becomes -2 as it approaches the equator.

Model meridional kinetic energy spectra at various latitudes are shown in Fig. 2b. The most striking difference of the spectral distribution of meridional kinetic energy from that of zonal kinetic energy is that the former always shows a band of maximum values over the scales of the maximum baroclinic instability (KL, 1977; Pratt, 1977, Desbois, 1975). The GLAS model, in general, reproduces fairly well the meridional kinetic energy spectra. However, careful inspection shows that the meridional kinetic energy in the low-wavenumber regime is too small, and too large over the band of maximum values. In other words, the long waves have less north-south motion, while the most baroclinically unstable waves have too strong north-south motion. The model westward moving waves have more meridional kinetic energy than the model eastward moving waves at the equator. The slope of meridional energy spectra in the high-wavenumber regime is close to -3, but the slope becomes -2 near the equator. Furthermore, the comparison between the zonal and meridional kinetic energy spectra shows that the energy content of eastward moving waves in the high-wavenumber regime of meridional kinetic energy spectra is larger than those of zonal kinetic energy spectra, except at 2°N and 58°S.

In order to compare the time characteristics of

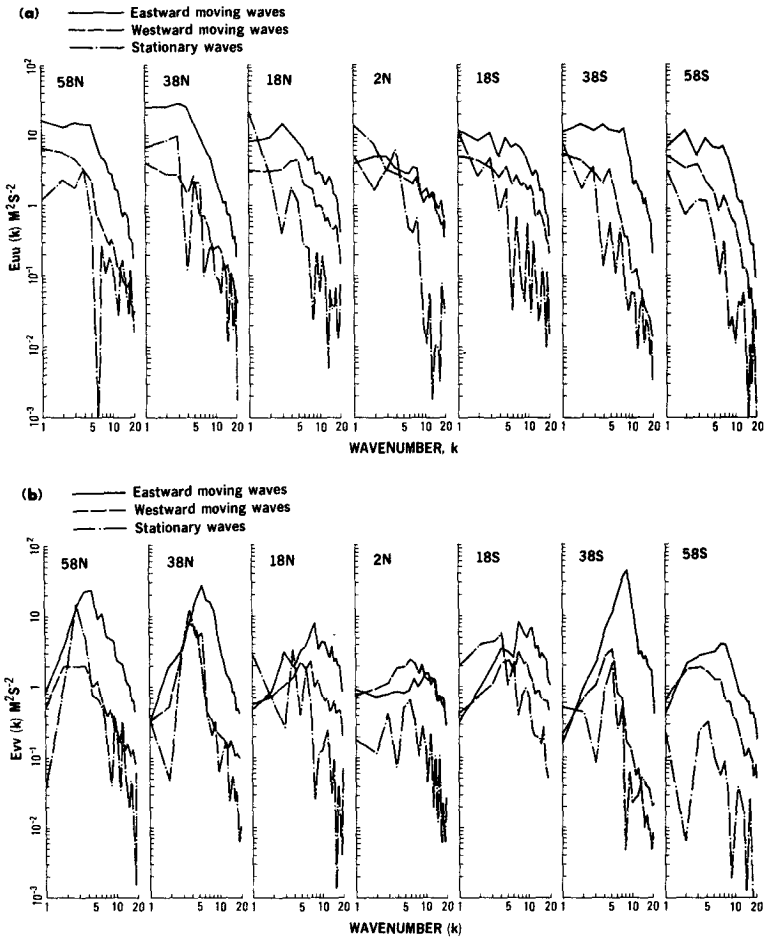

FIG. 2. Wavenumber spectra of (a) zonal and (b) meridional kinetic energy of the GLAS model at 200 mb and various latitudes.

model disturbances with the observational study of KL, the frequency spectra of zonal and meridional motion of the eastward and westward motion at 200 mb of the GLAS model are shown in Fig. 3. There is no pronounced difference between the frequency spectra of zonal and meridional motion as the wavenumber spectra of these two motions. The spectra of the eastward moving waves have larger energy content than the westward moving waves, except some low-frequency components of zonal motion at 58°N and intermediate-frequency disturbances of meridional motion at 2°N. The difference of frequency spectra between eastward and westward motions decreases as it approaches the equator. Furthermore, the spectra decrease as the frequency increases. These general features of frequency spectra are similar to KL's analysis. Notice that some differences exist between KL's and the model results. The model frequency spectra of eastward moving waves have a band of large values between 5 and 20 cycles (90 days)$^{-1}$ in the middle and high latitudes of the NH and 38°S. The most distinct feature is that the eastward moving waves peak at 7 cycles (90 days)$^{-1}$ which has a period of 12.9 days in the frequency spectra of zonal motion at 58°N, 38°N, 18°N, and meridional motion at 58°N, 38°N and 38°S. In fact, Hayashi and Golder (1977) also find a 12-day wave in the zonal and meridional motion at 190 mb of the GFDL model. They interpret the 12-day disturbance as strong cyclones. Miller (1974) also shows a 14–15 day vacillation of atmospheric energy. In any event, this type of wave disturbance does not show in the KL observational analysis. Through careful comparison between the frequency spectra of KL and GLAS model, one finds that the low-frequency [<5 cycles (90 days)$^{-1}$] regime of the GLAS model has less energy than KL's observational spectra. Pratt (1979) also finds that both the GFDL and NCAR models in middle and high latitudes have less wave activity than the atmosphere in the planetary-scale wave domain of 1–3 week period. The frequency spectra of the GLAS model in the high-frequency regime follow a power law as KL's analysis. The slope of the model

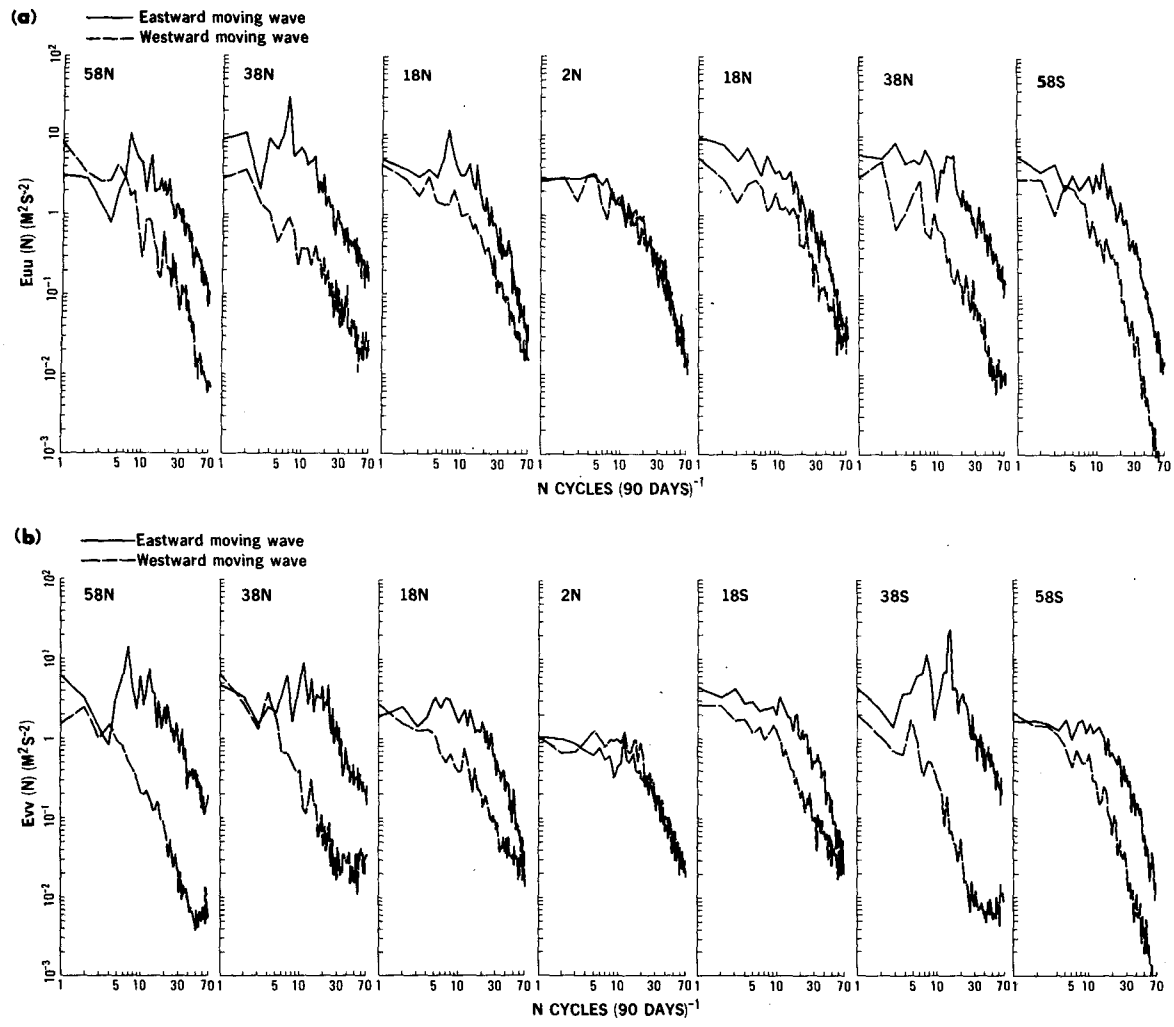

FIG. 3. As in Fig. 2 except for frequency spectra.

frequency spectra varies from −2 to −3, and −4 at 58°S for zonal motion. In other words, the frequency spectra of the GLAS model decrease faster with increasing frequency than the observation.

d. Wavenumber and frequency spectra of momentum transport

The general feature of the momentum transport in the wavenumber domain of the NH in the study of KL, and Hayashi and Golder (1977) is (i) the equatorial transport at high latitudes by stationary and transient waves of low-wavenumber regime; (ii) the poleward transport in middle latitudes by the planetary-scale stationary waves and baroclinically unstable transient waves; and (iii) the southward transport at the equator by planetary-scale stationary waves. The SH in Desbois' (1975) study shows a somewhat different picture: (i) the poleward transport in the middle latitudes is attributed to the baroclinically unstable waves and (ii) the equatorward transport at high latitudes is due to low-wavenumber waves.

The wavenumber cospectra of momentum transport of the GLAS model at 200 mb for various latitudes are shown in Fig. 4a. The momentum is transported equatorward at 58°N by wavenumber 4 and 5 of the stationary and eastward moving waves, while wavenumber 3 of the stationary wave transports momentum northward. The equatorward transport by wavenumber 2 of the stationary and eastward moving waves found by KL is not shown in the model. The poleward transport at 38°N is mainly accomplished by baroclinically unstable eastward moving waves and stationary wavenumber 3 and 5. Notice that the transport by baroclinically unstable eastward moving waves is much larger than the atmosphere in KL's analysis. The pronounced transports of stationary wavenumbers 1 and 5 of

the westward moving waves are missing in the model. The poleward transport at 18°N is weak and is attributed to stationary wave one and cyclone-scale eastward moving waves. The pronounced southward transport at the equator by stationary wavenumbers 2 and 4 of the KL analysis does not exist in the model, while the model stationary wavenumber 1 provides northward transport. Comparing the momentum transport in the SH of the GLAS model at 200 mb with Desbois' result, we can see that the maximum transport is attributed to the eastward moving wave 7 rather than wavenumber 5 as the observational study shows. In addition, the equatorward transport of momentum by the low wavenumber regime in Desbois' analysis disappears in the model. This transport is mainly contributed by the cyclone-scale eastward moving waves.

The frequency cospectra of momentum transport at high latitudes is mainly performed by eastward moving waves of low frequency. In middle latitudes, the momentum is mainly transported poleward by the eastward moving waves, especially those with a period of 5, 8 and 16 days, and by the westward moving waves of low frequency. The transport is not significant at the equator by the moving waves.

Except at the equator, the contribution to the model momentum transport by the westward moving waves is not significant over most frequencies. At 58°N, the equatorward transport is mainly executed by the eastward moving waves, especially with frequency 7 and 13 cycles (90 days)$^{-1}$, the eastward moving waves of low frequency transport the momentum poleward. In the middle latitudes and subtropics of the NH, the poleward transport of momentum is mainly carried out by the eastward moving waves with peak values at 7 and 11 cycles (90 days)$^{-1}$ at 38°N and seven cycles (90 days)$^{-1}$ at 18°N. The southward transport at the equator is more significant than observed and performed by the westward moving waves of low frequency especially 1, 4 and 8 cycles (90 days)$^{-1}$. In the middle latitudes and subtropics of the SH, the poleward transport of momentum is mainly provided by the eastward moving waves with frequency less than 20 cycles (90 days)$^{-1}$. The momentum transport is not significant at 58°S.

In summary, the momentum transport by the stationary waves of low wavenumber and the westward moving waves of low frequency are not simulated well by the GLAS model.

e. Wavenumber-frequency spectra of zonal and meridional kinetic energy, and momentum transport

It was mentioned in the introduction that two methods were employed to make spectral analysis of atmospheric motions, the lag-correlation method and the direct Fourier transform method. Hayashi and Golder (1977) and Pratt (1977) use the former method, while Kao and his colleagues (Kao and Wendell, 1970; Wendell, 1969; Kao *et al.*, 1970; Kao and Kuczek, 1973) use the latter method. The general finding of their wavenumber-frequency spectra of kinetic energy and momentum is the following. In the middle latitudes, the preferred spectral band is oriented from low wavenumber, low frequency of westward moving waves to high wavenumber and high frequency of eastward moving waves. The wave motion of the atmosphere in the

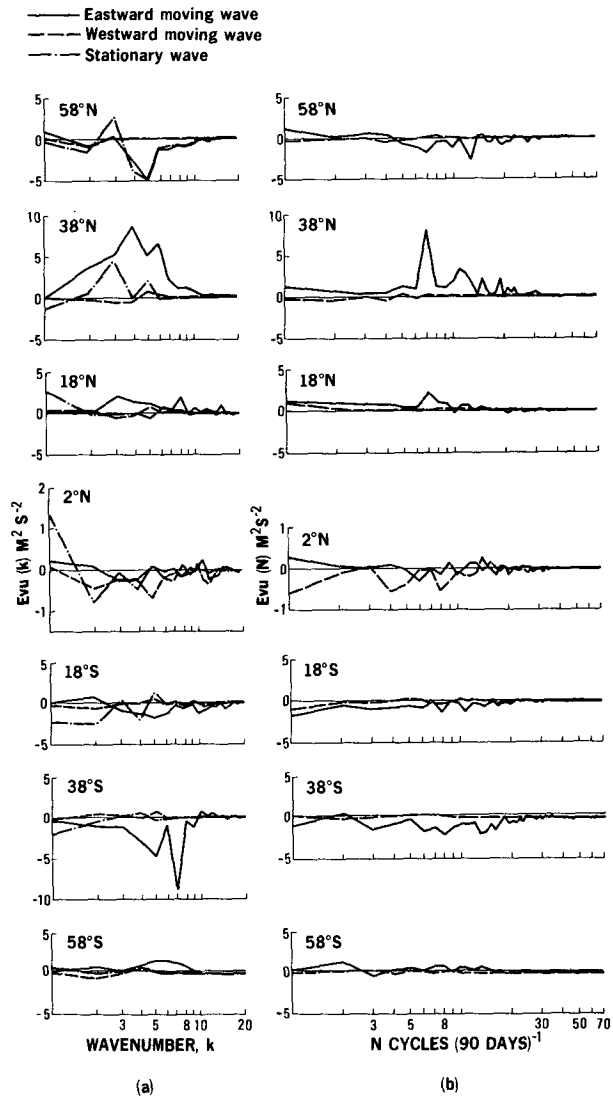

FIG. 4. (a) Wavenumber cospectra of momentum transport associated with stationary and moving waves of the GLAS model at 200 mb and various latitudes. (b) As in (a) except for frequency cospectra.

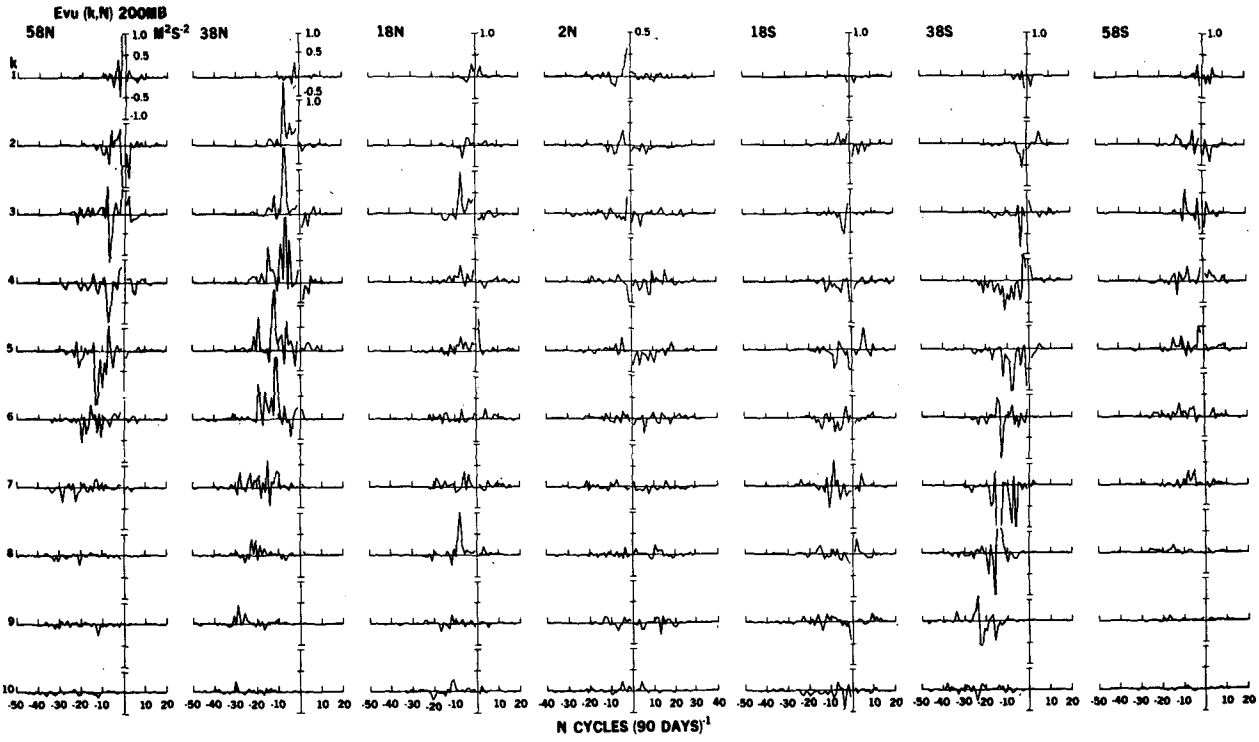

FIG. 5. Wavenumber-frequency spectra of zonal motion at 200 mb of the GLAS model.

dominant region of the spectral density is essentially of the Rossby type. In the tropics, the spectral band is oriented from low wavenumber and frequency to high wavenumber and low frequency.

Figs. 5–7 display the frequency-wavenumber spectra of zonal motion, meridional motion, and momentum transport at 200 mb and various latitudes of the GLAS model. The common features of these spectra is a preferred band that extends from a region of low wavenumber and low frequency of the westward moving waves to a region of high wavenumber and high frequency of the eastward moving waves in the middle and high latitudes in both hemispheres. The preferred band of spectra in the tropics extends from the region of low wavenumber and frequency to a region of high wavenumber and low frequency. These common features of the GLAS model spectra are similar to Kao's.

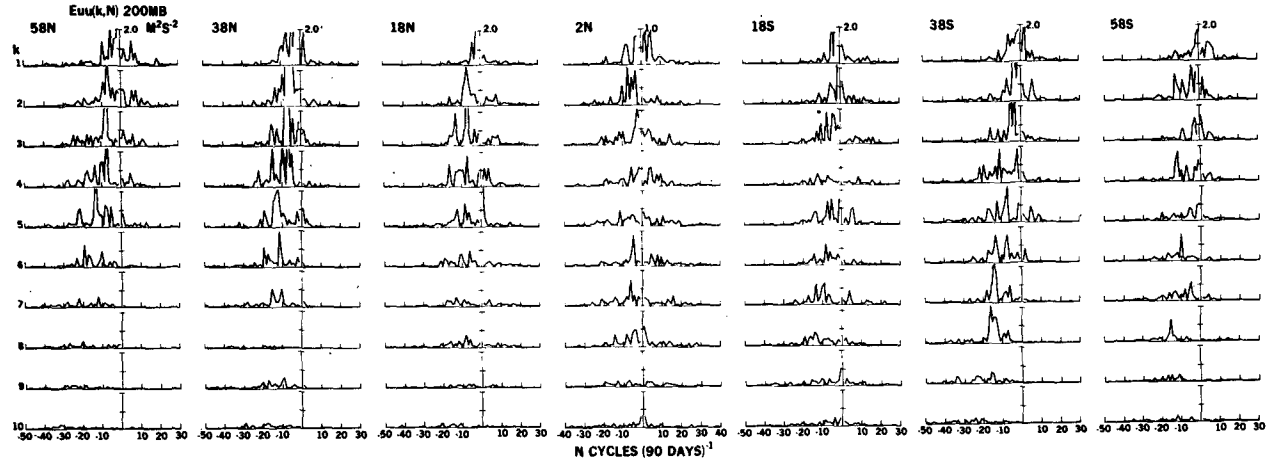

FIG. 6. Wavenumber-frequency spectra of meridional motion at 200 mb of the GLAS model.

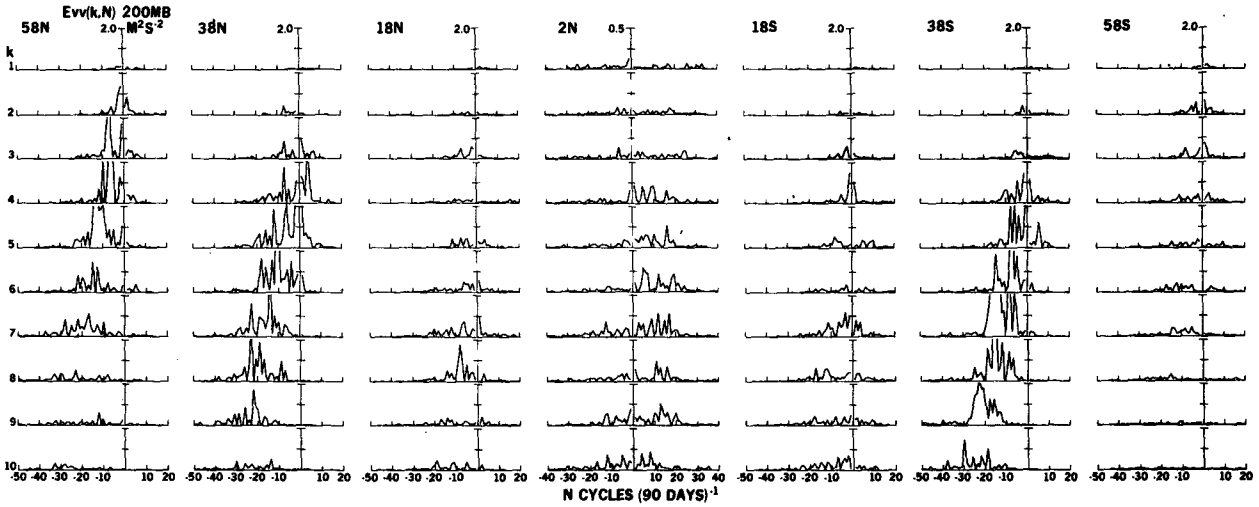

FIG. 7. Wavenumber-frequency cospectra of momentum transport at 200 mb of the GLAS model.

The contrast of zonal spectra in both hemispheres shows that the Northern Hemisphere has higher wave activities. This is expected because the climate run of present analysis is the late winter and early spring. The maximum values of spectra at 38°N and 58°N occur at wavenumbers 3 and 4 with frequency of seven cycles (90 days)$^{-1}$. Notice that wavenumbers 7 and 8 with frequency of 15 cycles (90 days)$^{-1}$ at 38°S has a significant power signal which does not appear in the Northern Hemisphere.

The meridional spectra show that the maximum spectral values are wavenumber 6 with frequency 10 cycles (90 days)$^{-1}$ at 38°N and wavenumber 8 with frequency of 15 cycles (90 days)$^{-1}$ at 38°S. In addition, the westward moving waves at the equator have higher power than the eastward moving waves. This is also consistent with the analysis of Kao and Kuczek (1973).

The comparison between zonal and meridional spectra shows that the maximum spectral values of the former spectra appear in the lower wavenumber than that of the latter spectra. In addition, the contrast between the spectra in both hemispheres shows that the maximum spectral values in the NH appear in the lower wavenumber, while they appear in the higher wavenumber in the SH. The same situation also applies to the spectra of momentum transport.

The spectra of momentum transport show significant northward transport at 38°N and significant southward transport at 38°S. The maximum values of spectra exists at wavenumber 4 with a frequency of 7 cycles (90 days)$^{-1}$ at 38°N and wavenumber 7 with a frequency of 15 cycles (90 days)$^{-1}$. The interhemispheric contrast of zonal and meridional spectra also applies to the spectra of momentum transport.

3. Diagnosis of nonlinear interactions of large-scale moving waves

a. Formation and computations

The diagnosis of nonlinear interactions of the moving waves in the GLAS model will be analyzed in terms of the kinetic energy equations of zonal and meridional motions and the momentum flux equation. The derivation of these equations in the wavenumber-frequency domain can be found in Kao (1968). The classification of wavenumber-frequency domain in the practical computations follow KL. Therefore, a brief description of the formulation and computations here should be sufficient.

The kinetic energy equations of zonal and meridional motions and the momentum flux equation in the physical domain can be expressed as

$$\frac{1}{2}\frac{\partial u^2}{\partial t} = \underbrace{-\frac{u^2}{a\cos\phi}\frac{\partial u}{\partial \lambda}}_{\text{(u1)}} \underbrace{-\frac{uv}{a}\frac{\partial u}{\partial \phi}}_{\text{(u2)}} + \underbrace{\frac{\tan\phi}{a}u^2v}_{\text{(u3)}} + \underbrace{fu(v - v_g)}_{\text{(u4)}} + \underbrace{uF_1}_{\text{(u5)}}, \quad (5)$$

$$\frac{1}{2}\frac{\partial v^2}{\partial t} = \underbrace{-\frac{uv}{a\cos\phi}\frac{\partial v}{\partial \lambda}}_{\text{(v1)}} \underbrace{-\frac{v^2}{a}\frac{\partial v}{\partial \phi}}_{\text{(v2)}} \underbrace{-\frac{\tan\phi}{a}u^2v}_{\text{(v3)}} \underbrace{-fv(u - u_g)}_{\text{(v4)}} + \underbrace{vF_2}_{\text{(v5)}}, \quad (6)$$

$$\frac{\partial}{\partial t}(vu) = -\frac{u}{a\cos\phi}\frac{\partial}{\partial t}(vu) \quad \text{(vu1)}$$

$$-\frac{v}{a}\frac{\partial}{\partial \phi}(vu) \quad \text{(vu2)} \qquad -\frac{\tan\phi}{a}u(u^2 - v^2) \quad \text{(vu3)}$$

$$-f[u(u - u_g) - v(v - v_g)] \quad \text{(vu4)} \qquad + vF_1 + uF_2. \quad \text{(vu5)} \quad (7)$$

The notations used are conventional. Let us use capital letters to designate the Fourier coefficients of atmospheric variables, Eqs. (5)–(7) in the wave-number-frequency domain can be written in the form (Kao, 1968):

$$|U(k,n)|^2 = \frac{T}{2\pi}\Big\{U(-k,-n)\frac{i}{n}\sum_j\sum_m\Big[\frac{i}{a\cos\phi}jU(j,m)U(k-j,n-m)\Big] \quad \text{(EUU)} \quad \text{(U1)}$$

$$-U(-k,-n)\frac{i}{na}\sum_j\sum_m[U_\phi(j,m)V(k-j;n-m)] \quad \text{(U2)}$$

$$-U(-k,-n)i\frac{\tan\phi}{na}\sum_j\sum_m[U(j,m)V(k-j,n-m)] \quad \text{(U3)}$$

$$-U(-k,-n)\frac{i}{n}f[V(k,n) - V_g(k,n)] \quad \text{(U4)} \qquad -\frac{i}{n}U(-k,-n)G_1(k,n)\Big\}, \quad \text{(U5)} \quad (8)$$

$$|V(k,n)|^2 = \frac{T}{2\pi}\Big\{V(-k,-n)\frac{i}{n}\sum_j\sum_m\frac{i}{a\cos\phi}[jV(j,m)U(k-j,n-m)] \quad \text{(EVV)} \quad \text{(V1)}$$

$$+V(-k,-n)\frac{i}{na}\sum_j\sum_m[V_\phi(j,m)V(k-j,n-m)] \quad \text{(V2)}$$

$$+V(-k,-n)\frac{i\tan\phi}{na}\sum_j\sum_m[U(j,m)U(k-j,n-m)] \quad \text{(V3)}$$

$$+V(-k,-n)\frac{i}{n}f[U(k,n) - U_g(k,n)] \quad \text{(V4)} \qquad -\frac{i}{n}V(-k,-n)G_2(k,n)\Big\}, \quad \text{(V5)} \quad (9)$$

$$E_{uv}(k,n) = \frac{T}{2\pi a}\Big\{\frac{-1}{\cos\phi}\frac{1}{n}\sum_j\sum_m jU(k-j,n-m)[U(j,m)V(-k,-n) + V(j,m)U(-k,-n)] \quad \text{(VU1)}$$

$$+\frac{i}{n}\sum_j\sum_m V(k-j,n-m)[U_\phi(j,m)V(-k,-n) + V_\phi(j,m)U(-k,-n)] \quad \text{(VU2)}$$

$$+\frac{i}{n}\tan\phi\sum_j\sum_m U(j,m)[U(-k,-n)U(k-j,n-m)-V(-k,-n)V(k-j,n-m)]\Big\}$$

(VU3)

$$+\frac{ifT}{2\pi n}\{U(-k,-n)[U(k,n)-U_g(k,n)]-V(-k,-n[V(k,n)-V_g(k,n)]\}$$

(VU4)

$$+\frac{T}{2\pi n}U(-k,-n)G_2(k,n)-V(-k,-n)G_1(k,n). \quad (10)$$

(VU5)

The left-hand sides of (8)–(10) are kinetic energy of zonal and meridional velocity, and momentum flux of moving waves with wavenumber k and frequency n, respectively. For convenience of future discussion, particular notations are designated to every term on the right-hand side of these equations. ( )1 and ( )2 represent the longitudinal and latitudinal convergence of either energy or momentum flux, respectively, by nonlinear interactions. ( )3 is sphericity effect and ( )4 + ( )5 is a combination of the ageostrophic effect, friction and computational errors. This combining effect can be determined by the residual method.

Every nonlinear interaction term on the right-hand side of (8) to (10) has a double summation which involves wavenumber and frequency. Following Kao's analysis, the range of wavenumber and frequency in the computation of this study covers $-20 \leqslant j \leqslant 20$ and $-90 \leqslant m \leqslant 90$. Since a great number of possible interactions is involved in these computations, Kao's classification of the wavenumber-frequency space into some particular domains is also adopted for the purpose of analysis. Tables 1 and 2 show the classifications of wavenumber and frequency, respectively.

Notice that the classification shown in Tables 1 and 2 can provide 28 domains and 406 possible interactions. A combination of a wavenumber and frequency classification represents a domain, for example, (k_s, n_l) designates the domain of long waves moving eastward with low frequency. The interactions are specified by placing the wavenumber-frequency domains side by side, e.g., $(k_s, n_m)(k_m, -n_l)$.

TABLE 1. Wavenumber classification.

Wavenumber k	Classification	Symbol
0	zonally averaged flow	0
1–5	long waves (small wavenumber)	k_s
6–9	medium waves	k_m
10–20	short waves (large wavenumber)	k_l

b. Diagnosis of spectral energy of moving waves

Wendell (1969) and sequential studies of Kao and collaborators have shown that the sum of the spectral energy of six wavenumber-frequency categories shown in Table 3 can explain most of the kinetic energy associated with moving waves. In order to examine how the nonlinear interactions contribute to spectral kinetic energy of model moving waves, only these six categories of moving waves will be analyzed using Eqs. (8) and (9). The contributions of various interactions for various latitudes at 200 mb of the GLAS model are shown in Table 3.

It is of interest to point out that EUU and EVV of long waves shown in Table 3 possess more spectral energy in the Northern Hemisphere, while medium waves have more spectral energy in the Southern Hemisphere. The longitudinal convergences of kinetic energy flux, U1 and V1, over the model globe give positive contribution to kinetic energy of eastward moving waves, but negative contribution to kinetic energy of the westward moving waves. The function of U1 and V1 at the equator at 200 mb of the GLAS model is opposite to that of KL's observational analysis at 500 mb where U1 and V1 extract kinetic energy from eastward moving waves and supply to westward moving waves. The disappearance of the easterly flow in the model equatorial area shown in Section 2b may cause the reversal of longitudinal convergence of kinetic

TABLE 2. Frequency classification.

Frequency n [cycles (90 days)$^{-1}$]	Period (days)	Classification (frequency)	Direction of wave motion	Symbol
−90 to −31	1–3	high	west to east	$+n_h$
−30 to −11	3–9	medium	west to east	$+n_m$
−10 to −1	9–90	low	west to east	$+n_l$
0		zero	stationary	0
1 to 10	9–90	low	east to west	$-n_l$
11 to 30	3–9	medium	east to west	$-n_m$
31 to 90	1–3	high	east to west	$-n_h$

energy flux at 200 mb of the GLAS model. It also is of interest to point out that UI and VI of long waves are very significant in the NH, but those of medium waves are generally significant in the SH. This feature is consistent with the latitudinal distribution of EUU and EVV.

The latitudinal convergence of kinetic energy flux, U2 and V2, is generally smaller than U1 and V1, especially the contrast between V1 and V2. Furthermore, U2 and V2 are not exactly of opposite sign to U1 and V1 as KL found at the 500 mb analysis. In fact, the signs of U2 and V2 are randomly distributed to some extent. The sphericity effect, U3 and V3, is generally very small and is essentially zero near the equator.

The residual term, (U4 + U5) and (V4 + V5), which is a combination of the ageostrophic effect, friction and computational error, is the same order of magnitude as U1 and V1. However, (U4 + U5) and (V4 + V5) have the opposite contribution to the spectral energy of moving waves as compared with U1 and V1. In other words, (U4 + U5) and (V4 + V5) give positive contribution kinetic energy to westward moving waves and negative contribution kinetic energy from eastward moving waves over the whole model globe, except for the eastward moving waves with medium frequency at some latitudes. Notice that the function of (U4 + U5) and (V4 + V5) also is opposite to KL's finding at the equator where KL found that (U4

TABLE 3. Linear and nonlinear contributions to energy spectra in various wavenumber-frequency domains at various latitudes at 200 mb.

		EUU =	U1	+ U2	+ U3	+ (U4 + U5)	EVV =	V1	+ V2	+ V3	+ (V4 + V5)
(k_s, $+n_l$)	58°N	15.25 =	104.67	+ 15.50	− 3.11	− 101.81	28.55 =	143.96	− 4.28	− 16.50	− 94.03
	38°N	45.85 =	345.70	− 61.87	− 9.09	− 228.98	8.60 =	201.85	+ 4.18	− 8.60	− 188.83
	18°N	18.25 =	40.99	+ 10.64	+ 0.20	− 33.58	4.29 =	15.86	− 0.20	+ 3.13	+ 14.00
	2°N	11.67 =	5.79	+ 14.35	+ 0.01	− 8.47	0.90 =	1.07	+ 0.43	+ 0.01	+ 0.61
	18°S	20.36 =	46.14	+ 90.72	+ 0.19	− 116.69	2.91 =	12.22	− 1.38	+ 0.71	− 8.64
	38°S	37.97 =	243.63	+ 40.24	+ 1.72	− 247.05	9.36 =	132.73	+ 6.66	+ 3.09	− 133.12
	58°S	18.59 =	90.82	+ 20.54	− 3.58	− 89.18	5.28 =	32.19	− 3.95	− 7.88	− 15.08
(k_s, $-n_l$)	58°N	16.53 =	−68.76	+ 1.26	+ 2.26	+ 81.77	5.32 =	−49.06	+ 9.66	+ 3.04	+ 41.68
	38°N	11.20 =	−113.16	− 2.86	+ 8.29	+ 118.43	9.19 =	−257.42	+ 6.48	+ 14.80	+ 245.33
	18°N	9.14 =	−20.82	+ 12.15	− 0.35	+ 18.17	1.67 =	−13.00	+ 0.51	− 1.40	+ 15.56
	2°N	7.62 =	−25.47	+ 0.88	+ 0.01	+ 32.20	1.75 =	−1.42	− 0.02	+ 0.03	+ 3.16
	18°S	8.44 =	−12.00	− 15.79	− 0.27	+ 36.30	3.08 =	−1.98	+ 0.13	+ 0.03	+ 5.02
	38°S	7.75 =	−60.11	− 37.90	+ 2.57	+ 103.19	2.64 =	−52.73	+ 2.83	+ 3.67	+ 48.87
	58°S	8.57 =	−20.85	− 3.14	− 1.68	+ 34.24	7.95 =	−8.80	+ 0.59	− 5.55	+ 21.71
(k_s, $+n_m$)	58°N	13.66 =	25.94	+ 2.00	− 2.79	− 11.49	12.66 =	32.51	+ 1.10	− 4.93	− 16.02
	38°N	21.18 =	48.64	+ 6.48	− 1.26	− 32.68	6.72 =	18.02	+ 0.11	− 2.02	− 9.39
	18°N	11.00 =	6.97	− 4.04	− 0.03	+ 8.04	1.40 =	0.95	+ 0.05	+ 0.13	+ 0.27
	2°N	4.48 =	1.02	− 1.87	− 0.00	+ 5.33	1.05 =	0.02	− 0.02	+ 0.00	+ 1.50
	18°S	8.31 =	3.57	+ 1.65	− 0.03	+ 3.11	0.75 =	0.30	+ 0.06	+ 0.08	+ 0.31
	38°S	12.28 =	24.71	− 1.48	+ 0.08	− 11.03	2.74 =	5.66	− 0.29	+ 0.14	− 2.77
	58°S	9.02 =	6.04	+ 1.41	+ 0.01	+ 1.56	1.43 =	2.67	+ 0.26	− 0.53	− 0.97
(k_m, $+n_l$)	58°N	2.50 =	29.10	− 2.10	− 0.45	− 24.05	5.52 =	38.30	− 1.11	− 2.56	− 29.11
	38°N	4.24 =	61.98	− 12.76	− 5.83	− 39.16	11.20 =	132.92	− 1.14	− 12.13	− 106.45
	18°N	4.81 =	19.08	+ 9.83	+ 0.14	− 24.24	4.23 =	31.00	+ 0.58	+ 0.30	− 27.65
	2°N	4.49 =	5.53	+ 1.84	− 0.00	− 2.88	1.06 =	2.36	− 0.43	− 0.01	− 0.88
	18°S	6.36 =	31.79	− 9.91	− 0.41	− 15.11	6.53 =	83.40	+ 3.67	− 0.57	− 49.97
	38°S	4.97 =	67.95	+ 14.27	− 7.91	− 69.34	25.52 =	182.32	+ 7.73	− 15.89	− 148.64
	58°S	3.13 =	20.00	− 1.06	− 1.05	− 14.76	4.67 =	19.71	− 0.16	− 2.46	− 12.42
(k_m, $-n_l$)	58°N	0.64 =	−8.71	− 4.91	− 0.43	+ 14.69	1.38 =	−13.45	+ 0.35	− 0.41	+ 14.89
	38°N	1.02 =	−39.01	− 5.03	+ 2.61	+ 39.20	0.87 =	−45.67	+ 3.28	+ 4.85	+ 38.41
	18°N	2.83 =	−9.25	+ 10.47	− 0.14	+ 1.75	0.97 =	−28.69	− 2.71	− 0.42	+ 32.78
	2°N	3.00 =	−3.55	+ 2.59	+ 0.00	+ 3.96	1.92 =	−2.12	− 0.69	− 0.02	+ 4.75
	18°S	3.48 =	−12.96	+ 8.80	+ 0.63	+ 7.01	3.92 =	−21.17	− 2.24	+ 1.12	+ 26.21
	38°S	13.89 =	−27.90	+ 9.65	+ 2.33	+ 29.81	0.74 =	−33.65	+ 3.22	+ 4.43	+ 26.94
	58°S	1.57 =	−5.82	+ 2.12	+ 0.07	+ 5.20	0.88 =	8.30	+ 0.53	+ 0.79	+ 7.86
(k_m, $+n_m$)	58°N	5.33 =	17.79	− 1.04	− 1.33	− 12.75	15.42 =	39.20	+ 0.88	− 2.90	− 21.76
	38°N	8.56 =	41.13	− 0.48	− 2.84	− 29.25	18.02 =	121.53	− 0.12	− 6.43	− 96.96
	18°N	6.25 =	7.90	− 3.10	+ 0.10	+ 1.35	5.14 =	5.86	− 0.00	+ 0.09	− 0.81
	2°N	2.39 =	1.22	− 0.11	− 0.00	+ 1.28	1.15 =	0.87	− 0.02	− 0.00	+ 0.30
	18°S	9.28 =	6.98	+ 0.13	+ 0.09	+ 2.08	7.10 =	6.76	+ 0.30	+ 0.15	− 0.11
	38°S	12.91 =	61.08	+ 3.25	− 5.85	− 45.57	64.70 =	192.48	− 0.35	− 11.04	− 116.39
	58°S	7.63 =	16.01	− 0.49	− 0.91	− 6.98	3.43 =	8.92	− 0.11	− 1.63	+ 1.74

+ U5) and (V4 + V5) supply kinetic energy to both eastward and westward moving waves.

Based upon their analysis for the linear and nonlinear interactions in spectral kinetic energy equations, KL proposed a scheme for the maintenance of spectral energy of moving waves in the westerly regime of the middle latitudes, shown in Fig. 8, and in the easterly regime of the tropics. Although U2 and V2 of the GLAS model at 200 mb do not show such a regularity as KL found in their analysis, KL's scheme for the diagnosis of spectral energy of moving waves in the westerly regime is in general applicable to the moving waves of the GLAS model at 200 mb.

It is also of interest to point out that our further examination on the contributions of various interactions to the spectral energy of moving waves reveals that the primary nonlinear interactions (not shown) are due to those involving the mean zonal flow with the long and medium waves of low and intermediate frequency. Our analysis in Section 2b shows that the model stationary waves are weak. KL found that the stationary waves play an important role in the nonlinear interactions. However, the present study shows that the role played by the model stationary waves is not vital.

c. *Diagnosis of spectral momentum transport flux of moving waves*

Eq. (9) is used to examine how the spectral momentum transport flux of moving waves is balanced through nonlinear interactions for various wavenumber-frequency domains and various latitudes. The resultant values of various interactions for the six wavenumber-frequency categories described in Section 3b are displayed in Table 4.

The spectral flux of momentum in various wavenumber-frequency domains shown in Table 4 directs toward north at 38°N, 18°N and 58°S, but toward south at 58°N, 2°N, 18°S and 38°S. The exception occurs to the low-frequency westward moving waves of long wavelength at 38°N where these waves present the southward transport of momentum flux.

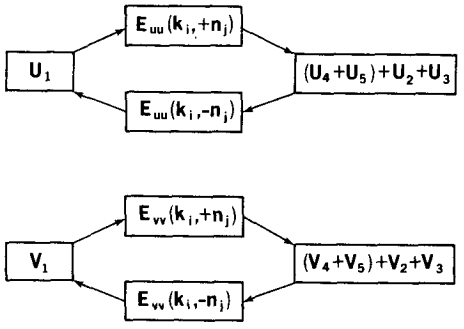

FIG. 8. Schematic diagram for maintenance of spectral energy of moving waves at 200 mb of the GLAS model.

TABLE 4. Linear and nonlinear contributions to northward momentum transport spectra in various wavenumber-frequency domains at various latitudes at 200 mb.

		EVU	=	VU1	+	VU2	+	VU3	+	(VU4 + VU5)
(k_s, $+n_l$)	58°N	−1.99	=	30.55	+	65.08	−	2.58	−	94.76
	38°N	19.25	=	184.04	−	2.35	−	1.67	−	110.77
	18°N	8.19	=	30.25	−	2.67	−	0.82	−	18.57
	2°N	−1.54	=	3.81	+	6.42	+	0.04	−	11.81
	18°S	−3.24	=	−9.09	+	12.22	+	2.11	−	8.98
	38°S	−10.75	=	−100.28	−	16.21	+	0.47	+	105.27
	58°S	6.55	=	51.90	−	0.05	+	3.61	−	48.91
(k_s, $-n_l$)	58°N	−1.32	=	−24.89	−	16.84	+	1.62	+	38.79
	38°N	−0.71	=	80.48	−	7.15	+	12.12	−	86.16
	18°N	1.60	=	−9.50	−	8.95	−	0.92	+	20.97
	2°N	−1.67	=	2.32	+	8.73	−	0.00	−	12.72
	18°S	−0.76	=	2.24	−	27.55	−	0.23	+	24.78
	38°S	−0.01	=	−13.08	−	8.11	+	2.31	+	18.87
	58°S	1.19	=	2.05	+	11.61	−	0.34	−	12.13
(k_s, $+n_m$)	58°N	−6.99	=	−15.07	+	4.11	−	2.58	+	6.55
	38°N	27.51	=	27.16	+	0.26	−	1.44	+	1.53
	18°N	7.37	=	0.34	+	1.03	+	0.02	+	5.92
	2°N	−1.64	=	0.14	−	0.58	+	0.00	−	1.20
	18°S	−4.13	=	−0.86	+	0.19	+	0.01	−	3.47
	38°S	−15.20	=	−13.52	−	0.02	+	0.31	−	1.97
	58°S	7.65	=	0.96	+	1.09	−	0.18	+	5.78
(k_m, $+n_l$)	58°N	−7.34	=	1.85	+	9.44	−	0.08	−	18.55
	38°N	29.10	=	30.81	+	16.11	−	6.27	−	11.55
	18°N	10.27	=	17.35	+	1.77	+	0.36	−	9.21
	2°N	−2.03	=	−1.49	−	1.25	−	0.01	+	0.72
	18°S	−6.10	=	−7.92	+	6.36	−	0.09	+	4.45
	38°S	−18.40	=	−29.20	+	3.58	−	7.69	+	15.41
	58°S	10.89	=	16.44	−	4.02	−	0.48	−	1.05
(k_m, $-n_l$)	58°N	−7.47	=	7.95	+	6.15	−	0.75	−	20.82
	38°N	29.48	=	−33.61	+	29.48	+	1.84	+	31.77
	18°N	11.42	=	−7.70	+	16.27	+	0.09	+	2.76
	2°N	−2.79	=	1.44	−	2.14	+	0.00	−	2.09
	18°S	−6.04	=	−9.22	−	9.88	+	0.11	+	12.95
	38°S	−18.56	=	5.79	+	15.58	+	2.61	−	42.54
	58°S	12.22	=	−4.61	+	0.45	−	0.12	+	16.50
(k_m, $+n_m$)	58°N	−11.33	=	−9.06	+	1.26	−	1.22	−	2.31
	38°N	37.89	=	37.86	−	2.53	−	3.78	+	5.34
	18°N	12.10	=	0.26	+	0.99	+	0.27	+	10.58
	2°N	−2.77	=	0.15	+	0.57	−	0.00	−	3.03
	18°S	−8.12	=	−2.26	−	2.97	+	0.15	−	3.04
	38°S	−27.52	=	−32.02	+	9.39	−	5.25	+	0.36
	58°S	14.30	=	5.65	+	0.28	−	0.90	+	9.27

The longitudinal convergence of momentum transport, VU1, is still generally the dominant term, and its contribution on the momentum transport is more complicated than its counterpart of the zonal and meridional kinetic energy discussed in Section 3b. At 38°N (midlatitude) and 18°N (subtropics) VU1 gives positive contribution to the northward transport of momentum to the eastward moving waves, but negative contribution to the westward moving waves. However, the reversed process occurs at 38 and 18°S, except (k_s, $+n_l$) at 38°S and (k_s, $+n_l$) at 18°S. At the equator VU1 is generally small, but contributes to northward transport of momentum for both the westward and eastward moving waves. At high latitudes of the SH (58°S), VU1 behaves in a similar way as its

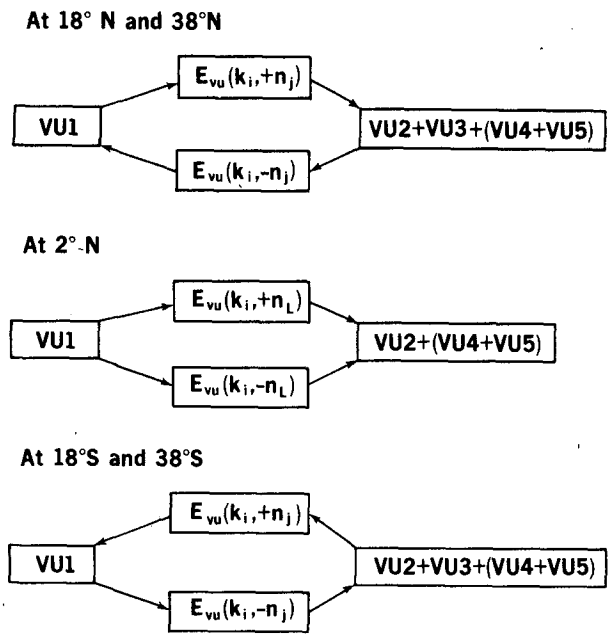

FIG. 9. Schematic diagram for maintenance of spectral momentum transport flux of moving waves at 200 mb of the GLAS model.

counterpart at the equator. However, VU1 at 58°N acts randomly as far as the direction of momentum transport is concerned.

The contribution of latitudinal convergence of momentum transport, VU2, is generally smaller than VU1, and is random. In some wavenumber-frequency categories at high latitudes (58°N) and low latitudes (2 and 18°N), VU2 becomes more significant than VU1. The effect of sphericity, VU3, is generally small and almost zero at 2°N. The residual term which involves the combination of the ageostrophic effect, frictional and computational errors, has the comparable magnitude with respect to VU1 and has an opposite sign except the wave categories belong to intermediate frequency domain.

In KL's scheme at 40°N, VU1 + VU3 give positive contribution to northward spectral momentum flux to the eastward moving waves, while VU2 + (VU4 + VU5) give negative contribution to northward spectral momentum flux from eastward moving waves. As for the westward moving waves, the contribution of VU1 + VU3 and VU2 + (VU4 + VU5) are reversed. At the equator, VU1 + VU2 give negative contribution to northward spectral momentum flux from both the eastward and westward moving waves, while (VU4 + VU5) give positive contribution to northward spectral momentum transport for both the eastward and westward moving waves. The comparison between Table 4 and KL's result shows that KL's scheme may not be applied to the GLAS model completely, especially at the equator where the easterlies do not show in the GLAS model. At 38 and 18°N of the GLAS model, we move VU3 to the group VU2 + (VU4 + VU5) and obtain the top diagram in Fig. 9. That is, VU1 gives positive contribution to northward spectral momentum flux for the eastward moving waves, while VU2 + VU3 + (VU4 + VU5) give negative contribution to northward spectral momentum flux for the eastward moving waves. The effect of VU1 and VU2 + VU3 + (VU4 + VU5) on the westward moving waves is opposite to that on the eastward moving waves. This scheme is reversed at 38 and 18°S. It is because the eddy transport of westerly momentum is south poleward. At the equator of the GLAS model, VU2 generally is larger than VU1 and is not so regular in sign. This does not show in KL's observational analysis. In order to compare with KL's study, we also modify KL's scheme at the equator by moving VU2 to (VU4 + VU5). The balance of spectral momentum flux at the equator of the GLAS model is opposite to KL's scheme in sign. In other words, VU1 gives positive contribution to northward spectral momentum transport to both eastward and westward moving waves, while VU2 + (VU4 + VU5) give negative contribution to northward spectral momentum transport for both eastward and westward moving waves.

It also should be pointed out that the detailed analysis of the contributions from various interactions to the spectral momentum transport (not shown) are those between the mean zonal flow and the long and medium waves with low and intermediate frequency. Again, the stationary waves do not play any significant role in nonlinear interactions.

4. Summary

The space-time Fourier spectral analysis and the equations of kinetic energy and momentum transport in the wavenumber-frequency domain proposed by Kao (1968) and modified by Kao and Lee (1977) using Tukey's numerical spectral analysis are employed to analyze the 200 mb wind fields of a 4-month climate experiment of the GLAS atmospheric circulation model. This climate run covers the period from 1 January to 30 April 1975. This study analyzes a 90-day (15 January–14 April 1975) wind field of this climate run. Comparison between the present study and observation, mainly Kao and Lee's (1977) study, leads to the following conclusions:

1) The 200 mb latitudinal distributions of model mean zonal wind, zonal and meridional kinetic energy and momentum transport of eddies agree fairly well with observations. However, some deficiencies of this climate run are revealed: equatorial easterlies disappear, and zonal kinetic energy and momentum transport of stationary waves are too small in the model Northern Hemisphere (NH).

2) The general features of wavenumber spectra of the model zonal and meridional kinetic energy for moving waves are consistent with observation. The model zonal kinetic energy in wavenumber one of stationary wave is too small in the NH subtropics and equator. Furthermore, the zonal kinetic energy of the model eastward moving waves in low-wavenumber regime is larger in NH and smaller in SH than observation. The meridional kinetic energy spectra of both hemispheres have smaller values in low-wavenumber regime and larger values in intermediate-wavenumber regime than observation.

3) The frequency spectra of zonal and meridional kinetic energy of eastward moving waves show a band [5 ~ 20 cycles (90 days)$^{-1}$] of large values in middle and high latitudes and peaks at 7 cycles (90 days)$^{-1}$ ~ 12.9 days. In addition, the frequency spectra have a slope of -2 to about -3 in a high-frequency regime, rather than -1 as Kao finds.

4) The model momentum transport in the wavenumber domain is mainly performed by the eastward moving and stationary waves of intermediate wavenumber in middle and high latitudes of the NH and only by the eastward moving waves of intermediate wavenumbers in middle and high latitudes of the SH. The southward momentum transport at the equator is due to the eastward moving waves of intermediate wavenumber. The momentum transport by the stationary waves of low wavenumber is too weak in the model. In the frequency domain, the momentum transport is principally carried by the eastward moving waves of 5 ~ 20 cycles (90 days)$^{-1}$ in both hemispheres, and 1 ~ 20 cycles (90 days)$^{-1}$ at 2°N. The momentum transport by the low-frequency waves is not significant in the model as found in observation.

5) The model wavenumber-frequency spectra of zonal and meridional motion and momentum transport have a preferred band which is oriented from low wavenumber and low frequency of the westward moving waves to high wavenumber and high frequency of eastward moving waves in middle and high latitudes. The preferred band of spectra in the tropics extends from low wavenumber and low frequency to high wavenumber and low frequency. Furthermore, maximum spectral value of zonal motion appears in lower wavenumber than that of meridional motion. These features of model wavenumber-frequency spectra are consistent with the spectral studies of Kao, Hayashi and Pratt. Another interesting feature of model spectra is that the maximum spectral value in NH occurs in lower wavenumber than in SH.

6) The mean westerlies exist over the whole model globe at 200 mb in this climate experiment. The nonlinear interactions by the longitudinal convergence of kinetic energy flux (U1 and V1) and a combination of ageostrophic effect and dissipation (U4 + U5) and (V4 + V5) are dominant and comparable. U1 and V1 give positive contribution to kinetic energy to the eastward moving waves, but give negative contribution to kinetic energy from the westward moving waves. (U4 + U5) and (V4 + V5) contribute oppositely as U1 and V1 do. The primary interactions of kinetic energy in wavenumber-frequency domain are largely through the interactions between mean zonal flow and the long and medium waves of low and medium frequencies. The significant role played by the stationary waves shown in Kao and Lee's does not appear in this model.

7) The contribution to momentum transport spectra by linear and nonlinear processes in the NH is similar to that of kinetic energy spectra. However, the contribution of longitudinal convergence of momentum transport flux (VU1) and a combination of ageostrophic effect and dissipation (VU4 + VU5) in SH is opposite to those in NH. At the equator, VU1 gives positive contribution to meridional flux of westerly momentum to both the eastward and westward moving waves, but VU4 + VU5 give negative contribution for both moving waves. This scheme is opposite to Kao and Lee's in direction. The primary interactions of meridional flux of westerly momentum is similar to those of kinetic energy.

Acknowledgments. Suggestions and discussions provided by Drs. S.-K. Kao, J. J. Tribbia, Y. Hayashi and David M. Straus were most helpful for the present study. We thank Dr. Milton Halem for his interest in this study. The constructive comments given by one of the anonymous reviewers are very helpful to clarify the presentation of this paper. The history tape of the GLAS atmospheric circulation model was prepared by Mr. William Byerly. This study is supported by NASA Grant NSG-5339.

REFERENCES

Arakawa, A., 1966: Computational design of long-term numerical integration of the equations of fluid motion: Two-dimensional incompressible flow. Part I. *J. Comput. Phys.*, **1**, 119–143.

Chen, T.-C., 1980: On the energy exchange between the divergent and rotational components of atmospheric flow over the tropics and subtropics at 200 mb during two northern summers. *Mon. Wea. Rev.*, **108**, 896–912.

Desbois, M., 1975: Large-scale kinetic energy spectra from Eulerian analysis of EOLE wind data. *J. Atmos. Sci.*, **32**, 1838–1847.

Halem, M., J. Shukla, Y. Mintz, M. L. Wu, R. Godbole, G. Herman and Y. Sud, 1979: Climate comparisons of a winter and summer numerical simulation with the GLAS general circulation model. *GARP Publ. Ser.*, **22**, 207–253.

Hayashi, Y., 1971: A generalized method of resolving disturbances into progressive and retrogressive waves by space Fourier and time cross-spectral analysis. *J. Meteor. Soc. Japan*, **49**, 125–128.

——, 1974: Spectral analysis of tropical disturbances appearing in a GFDL general circulation model. *J. Atmos. Sci.*, **31**, 180–218.

——, and D. G. Golder, 1977: Space-time spectral analysis of

mid-latitude disturbances appearing in a GFDL general circulation model. *J. Atmos. Sci.*, **34**, 237–262.

Kao, S.-K., 1968: Large-scale atmospheric motion and transports in frequency wavenumber space. *J. Atmos. Sci.*, **25**, 32–38.

——, and L. L. Wendell, 1970: The kinetic energy of the large-scale atmospheric motion in wavenumber-frequency space: I. Northern Hemisphere. *J. Atmos. Sci.*, **27**, 359–375.

——, and R. J. Kuczek, 1973: The kinetic energy of large-scale atmospheric motion in wavenumber-frequency space: III. The tropics. *J. Atmos. Sci.*, **30**, 308–312.

——, and H. N. Lee, 1977: The nonlinear interactions and maintenance of the large-scale moving waves in the atmosphere. *J. Atmos. Sci.*, **34**, 471–485.

——, C. Y. Tsay and L. L. Wendell, 1970: The meridional transport of angular momentum in wavenumber-frequency space. *J. Atmos. Sci.*, **27**, 614–626.

Krishnamurti, T. N., 1971: Tropical east–west circulations during the northern summer. *J. Atmos. Sci.*, **28**, 1342–1347.

——, K. Kanamitsu, W. J. Koss and J. D. Lee, 1973: Tropical east–west circulations during the northern winter. *J. Atmos. Sci.*, **30**, 780–787.

Manabe, S., J. Smagorinsky, J. L. Holloway, Jr., and H. M. Stone, 1970: Simulated climatology of a general circulation model with a hydrologic cycle. III. Effects of increased horizontal computational resolution. *Mon. Wea. Rev.*, **98**, 175–212.

Miller, A. J., 1974: Periodic variation of atmospheric circulation at 14–16 days. *J. Atmos. Sci.*, **31**, 720–726.

Morel, P., and M. Desbois, 1974: Mean 200-mb circulation in the Southern Hemisphere deduced from EOLE balloon flights. *J. Atmos. Sci.*, **31**, 394–407.

Pratt, R. W., 1976: The interpretation of space-time spectral quantities. *J. Atmos. Sci.*, **33**, 1060–1066.

——, 1977: Space-time kinetic energy spectral in mid-latitude. *J. Atmos. Sci.*, **34**, 1054–1057.

——, 1979: A space-time spectral comparison of the NCAR and GFDL general circulation models to the atmosphere. *J. Atmos. Sci.*, **36**, 1681–1691.

Straus, D. M., and J. Shukla, 1981: Space-time spectral structure of a GLAS general circulation model and a comparison with observations. *J. Atmos. Sci.*, **38** (May).

Tsay, C. Y., 1974a: A note on the methods of analyzing travelling waves. *Tellus* **26**, 412–415.

——, 1974b: Analysis of large-scale wave disturbances in the tropics simulated by an NCAR global circulation model. *J. Atmos. Sci.*, **31**, 330–339.

Tukey, J. W., 1967: Spectrum calculations in the new world of the fast Fourier transform. *Advanced Seminar on Spectral Analysis of Time Series*, B.

Webster, P. J., and D. G. Curtin, 1974: Interpretations of the EØLE experiment. I. Temporal variation of Eulerian quantities. *J. Atmos. Sci.*, **31**, 1860–1875.

Wellck, R., A. Kasahara, W. Washington and G. de Santo, 1971: Effect of horizontal resolution in a finite-difference model of the general circulation. *Mon. Wea. Rev.*, **99**, 673–683.

Wendell, L. L., 1969: A study of the large-scale atmospheric turbulent kinetic energy in wavenumber-frequency space. *Tellus*, **21**, 760–788.